Proceedings of Czech–Japanese Seminar in Applied Mathematics 2004
August 4-7, 2004, Czech Technical University in Prague
http://geraldine.fjfi.cvut.cz
pp. 165–175

NUMERICAL SIMULATION OF REACTION-DIFFUSION DYNAMICS

ROBERT STRAKA[1]

Abstract. Reaction-diffusion system Brusselator is theoretical model of nonlinear chemical reaction in stirred reactor tank. In the reaction scheme the initial components A and B are transformed into products D and E via the reaction intermediates X and Y. It is well known that this model exhibit various types of solutions depending on the characteristic length of reactor tank L. Keeping L small $L \in \langle 0, 0.513)$ we obtain trivial invariant set - stable fixed point. If L increases we obtain stable symmetic periodic solution - we crossed first Hopf bifurcation point $L^* = 0.513$. The branch of stable asymmetric solutions bifurcates in neighbourhood of $L^+ = 1.225$ and further develop to invariant torus. Developments of this torus were studied using methods of Poincaré intersection, it's fractal dimension and Lyapunov characteristic exponents. Symmetry of solutions and period of periodic solutions were studied as well.

Key words. Brusselator, reaction-diffusion equations, Poincaré intersection, fractal dimension, symmetry of solution, Lyapunov characteristic exponent.

AMS subject classifications. 35K55, 35K57, 37L30, 65N06, 65N40, 65P30

1. Introduction. This paper summarizes results of numerical simulation of parabolic equations of the Brusselator model. This model exhibits various types of dynamics which was investigated. The main goal of this paper is to characterize branches of stable periodic solutions and investigate development of invariant tori and their geometrical structure. Methods of Poincaré map, Lyapunov characteristic exponents (LCEs) and box-counting dimension of intersections were used. Symmetries of solution branches were studied as well to identify symmetry-breaking bifurcation points. I would like thank to Dr. Michal Beneš for important advices and helpful notes.

2. Brusselator RD model. Theoretical example of nonlinear chemical reaction in theory of dissipative structures, the Brusselator model. In the reaction scheme the initial components A and B are transformed into products D and E via the reaction intermediates X and Y.

$$\begin{aligned} \mathrm{A} &\xrightarrow{k_1} \mathrm{X}, \\ \mathrm{B} + \mathrm{X} &\xrightarrow{k_2} \mathrm{Y} + \mathrm{D}, \\ 2\mathrm{X} + \mathrm{Y} &\xrightarrow{k_3} \mathrm{X}, \\ \mathrm{X} &\xrightarrow{k_4} \mathrm{E}. \end{aligned}$$

For constant concentrations of components A and B, reaction rate constants $k_i = 1, \quad i = 1, 2, 3, 4$, isothermic conditions and one-dimensional case, resulting system of PDEs is as follows:

[1]Department of Mathematics, Faculty of Nuclear Sciences and Physical Engineering, Czech Technical University in Prague, Trojanova 13, 120 00 Prague, Czech Republic.

$$\frac{\partial x}{\partial t} = \frac{D_x}{L^2}\frac{\partial^2 x}{\partial z^2} + A - (B+1)x + x^2 y,$$
$$\frac{\partial y}{\partial t} = \frac{D_y}{L^2}\frac{\partial^2 y}{\partial z^2} + Bx - x^2 y$$

where D_x, D_y are diffusion rates[1], L is characteristic length of the reactor tank. In every numerical simulations homogeneous Dirichlet boundary conditions were used:

$$z \in \{0,1\}: \qquad x(z,t) = A, \quad y(z,t) = \frac{B}{A}.$$

and intial conditions:

$$x(z,0) = A + \sqrt{2}\sin(\pi z), \qquad y(z,0) = \frac{B}{A} + \sqrt{2}\sin(\pi z).$$

3. Used techniques. In several subsections, basics of techniques for investigation dynamics of RD systems are described. Mainly the technique of Poincaré intersection which is useful to reveal geometrical complexity of invariant torusoidal attractors.

3.1. Discretization of PDEs. Method of finite differences and method of lines were applied to the PDEs. Consider the RD system with Dirichlet boundary condition and mesh with equidistant step[2]:

$$z_i = ih, \quad i = 0,\ldots,n, \quad h = \frac{1}{n},$$

denote solution in mesh points as:

$$x_i(t) \sim x(z_i,t), \quad y_i(t) \sim y(z_i,t),$$

we approximate using central difference formulas $i = 1,\ldots,n-1$

$$\frac{\mathrm{d}x_i}{\mathrm{d}t} = \frac{D_x}{L^2h^2}(x_{i-1} - 2x_i + x_{i+1}) + A - (B+1)x_i + x_i^2 y_i,$$
$$\frac{\mathrm{d}y_i}{\mathrm{d}t} = \frac{D_y}{L^2h^2}(y_{i-1} - 2y_i + y_{i+1}) + Bx_i - x_i^2 y_i,$$

from boundary condition we obtain

$$x_0 = x_n = A, \quad y_0 = y_n = \frac{B}{A}.$$

Now we have system of $2(n-1)$ ODEs with $O(h^2)$ accuracy in space, which can be solved with the Runge-Kutta method (4th-order Merson's scheme was used with adaptive size of time step). In such way we can obtain $n-1$ orbit for each $x(z,t)$, $y(z,t)$ and apply techniques for dynamics investigation of given RD system.

3.2. Poincaré intersection. It is essential tool for investigation tori development. We define hypersurface Σ given by $S(x_1,\ldots,x_n) = 0$, which lies in the attractor $\mathcal{A}$ and intersects trajectory Γ (see Fig.3.2).
Integrating system of ODEs and evaluating sign of Σ yields the points of Poincaré mapping obtained by linear aproximation. Although linear approximation can produce numerical errors, the Hénon method was used and compared with those linear approximation intersections.

[1] In numerical experiments following parameter's values were used: $D_x = 0.008$, $D_y = 0.004$, $A = 2$, $B = 5.45$.

[2] In numerical experiments $n = 100$ was used, except of LCEs evaluation where $n = 20$ was used.

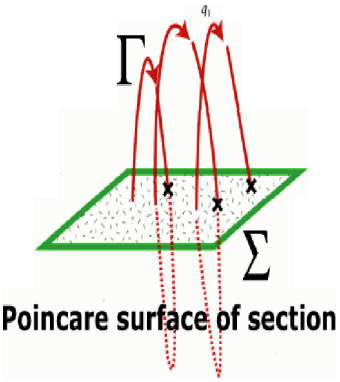

FIG. 3.1. *Poincaré intersection.*

3.2.1. The Hénon method. Simple form of $\Sigma \equiv x_i - a = 0$ is often used. We divide the system of ODEs by i-th equation provided $f_i(\mathbf{x}, \alpha) \neq 0$ in neighbourhood of Σ holds.

$$\begin{aligned} \frac{\mathrm{d}x_1}{\mathrm{d}x_i} &= \frac{f_1(\mathbf{x},\alpha)}{f_i(\mathbf{x},\alpha)}, \\ &\vdots \\ \frac{\mathrm{d}x_n}{\mathrm{d}x_i} &= \frac{f_n(\mathbf{x},\alpha)}{f_i(\mathbf{x},\alpha)}. \end{aligned} \tag{3.1}$$

Then we integrate the original system till Σ change its sign. By this point we integrate system (3.1) with step $\Delta x_i = x_i - a$. Such points lie on Σ with accuracy of integration method. After obtaining point of intersection we continue with integration of the original ODEs.

3.3. Symmetry of solutions, diagram of solutions. By changing L, symmetry of solutions can change. We define

$$x_{1/2}(t) = \int_0^{1/2} x(z,t)\mathrm{d}z, \qquad x_{2/2}(t) = \int_{1/2}^{1} x(z,t)\mathrm{d}z, \tag{3.2}$$

and plot them. Symmetric and asymmetric solutions are indicated by plots similar to those as in Fig.3.2. We use methods of Poincaré mapping to measure period of solutions. Diagram of periodic solutions is plot of solution's period (amplitude) against characteristic length of reactor tank L.

4. Numerical results. Following numerical results are introduced: diagram of solutions (Fig.4.1) with solutions plots for $x(z,t)$ and $y(z,t)$ (Fig.4.2), orbits (Fig.4.3) as well as symmetry plots (Fig.4.4) for points from each branch in diagram. Geometrical study of tori development follows in Fig.4.5 and comparison of linear approximation and the Hénon method (Fig.4.6). The last part is table of Lyapunov characteristic exponents and box-counting dimension of Poincaré intersections (Tab.5).

5. Conclusions. Dynamics of the Brusselator model was investigated, three branches of stable periodic solution were found (in range $L \in \langle 0, 2\rangle$), from first Hopf bifurcation point at $L = 0.513$ till $L \sim 1.225$ (symmetry-breaking bifurcation point)

L	λ_1	λ_2	λ_3	λ_4	$\dim_{box}$
0.3	−0.44	−2.39	−5.59	−9.97	-
1.0	0.00	−0.35	−0.45	−0.92	-
1.24	0.00	−0.20	−0.42	−0.75	-
1.3	0.00	−0.09	−0.38	−0.56	-
1.38	0.00	−0.03	−0.31	−0.52	1.08
1.42	0.00	−0.01	−0.28	−0.55	1.39
1.47	0.01	0.0	−0.24	−0.51	1.17
1.52	0.02	0.00	−0.22	−0.46	-
1.56	0.02	0.00	−0.22	−0.42	1.03
1.57	0.01	0.00	−0.22	−0.43	-
1.7	0.00	−0.02	−0.15	−0.31	-
1.75	0.00	−0.01	−0.21	−0.36	-
1.81	0.01	0.00	−0.20	−0.34	1.16
1.85	0.01	0.00	−0.01	−0.18	0.98
1.9	0.01	0.00	−0.15	−0.31	1.08
1.97	0.01	0.00	−0.15	−0.28	1.11
1.98	0.01	0.00	−0.14	−0.27	1.54
1.99	0.01	0.00	−0.13	−0.26	1.15
2.0	0.01	0.00	−0.13	−0.26	1.88

TABLE 5.1

Table of Lyapunov characteristic exponents and box-counting dimensions of Poincaré intersections. At least one positive LCE indicates invariant torus, zero LCE indicates periodic solution and whole negative LCEs stand for trivial invariant set–fixed point.

it is branch of stable symmetric periodic solutions. After symmetry-breaking bifurcation, branch of stable asymmetric periodic solutions exist and further develop to branch of invariant tori in neighbourhood of $L = 1.38$. Small part of stable, asymmetric, periodic solutions branch is also visible. Toruses were studied using techniques of Poincaré intersections to show great geometrical complexity of toroidal structures and to show development of these structures (torus doubling and deformation which lead to more complicated shapes). Comparison of two methods for Poincaré intersection prove that when linear approximation is used, some extra parts in the intersection can appear. Lyapunov characteristic exponents and box-counting dimension for Poincaré intersections clasifies type of the obtained solution.

Acknowledgment. Partial support of the project "Applied Mathematics in Technology and Physics" MSM 6840770010 of the Ministry of Education of the Czech Republic and of the project "Advanced Control and Optimization for Power Generation" No. 1H-PK/22 of the Ministry of Industry and Trade of the Czech Republic is acknowledged.

REFERENCES

[1] G. EDGAR. *Measure, Topology and Fractal Geometry*, Springer-Verlag, Berlin, 1989.
[2] M. HOLODNIOK, A. KLÍČ, M. KUBÍČEK AND M. MAREK. *Metody analýzy nelinearních dynamických modelů*, Academia, Praha, 1986.
[3] M. KUBÍČEK, M. MAREK AND P. RASCHMAN. *Concentration waves in reaction-diffusion systems*, Scientific papers of the Prague Institute of Chemical Technology, K 17 (1982),151-175.

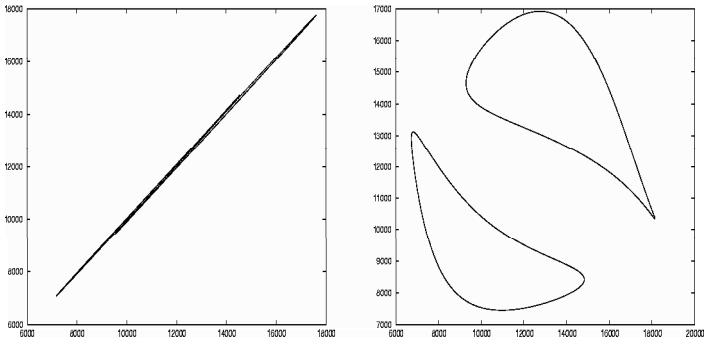

(a) Symmetry of solution (b) Asymmetry of solution

FIG. 3.2. *Characteristic plots of symmetric and asymmetric solutions.*

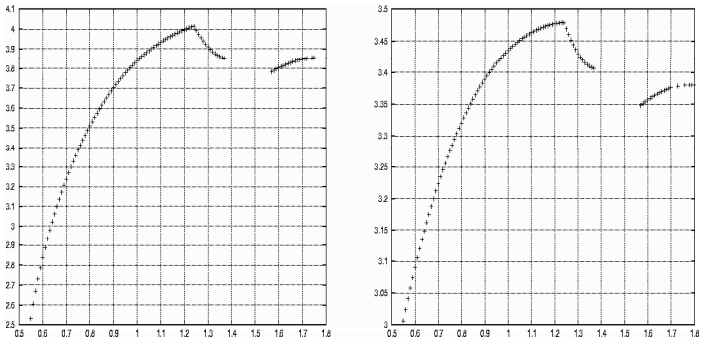

(a) Amplitude vs. L (b) Period vs. L

FIG. 4.1. *Diagrams of solutions for Brusselator model. Three branches of stable solutions are displayed.*

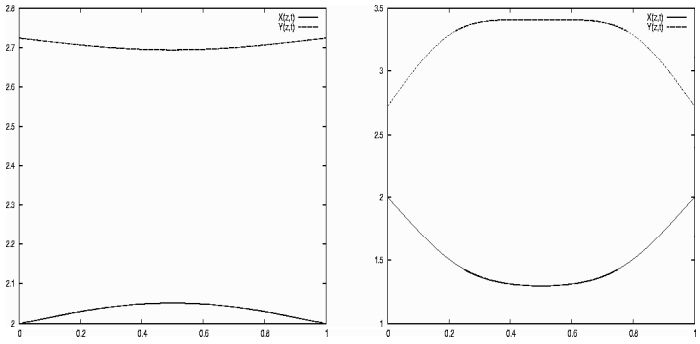

(a) $L = 0.3, \quad t = 0.05$ (b) $L = 1.0, \quad t = 5$

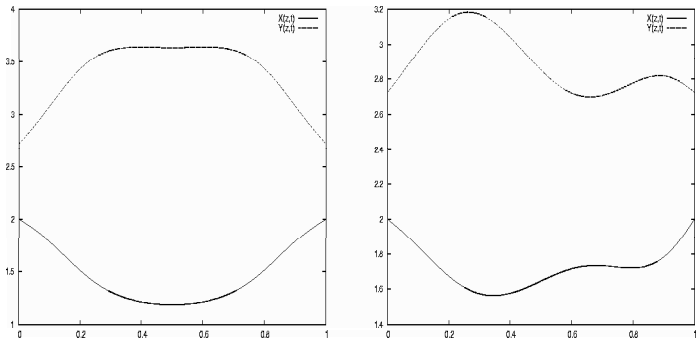

(c) $L = 1.24, \quad t = 5$ (d) $L = 1.3, \quad t = 50$

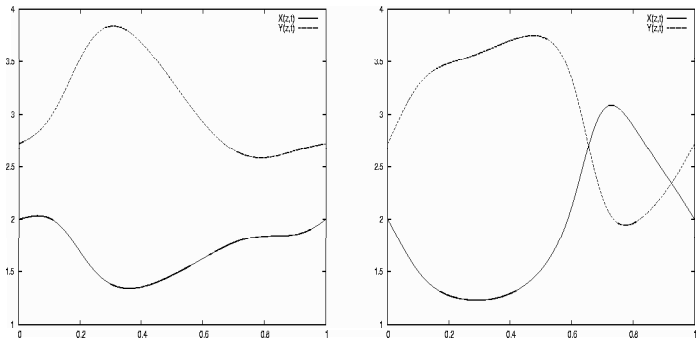

(e) $L = 1.57, \quad t = 50$ (f) $L = 1.7, \quad t = 50$

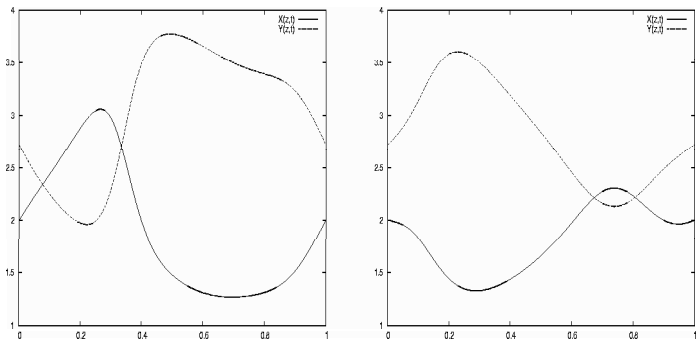

(g) $L = 1.75, \quad t = 50$ (h) $L = 1.98, \quad t = 50$

FIG. 4.2. *Solutions of concentrations intermediates X and Y in space, for several values of L and time t.*

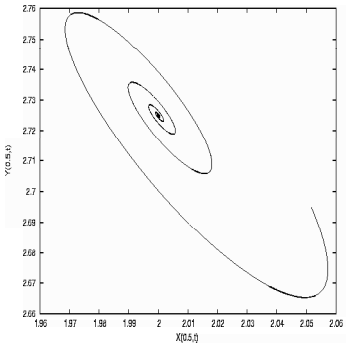

(a) $L = 0.3, \quad t \in \langle 0.05, 1 \rangle$

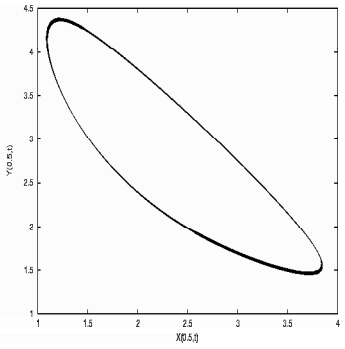

(b) $L = 1.0, \quad t \in \langle 0.5, 5 \rangle$

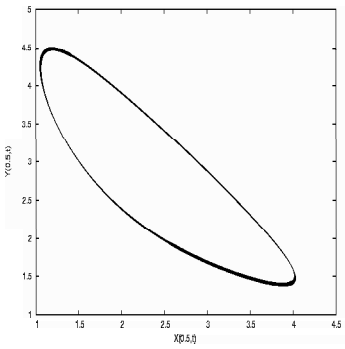

(c) $L = 1.24, \quad t \in \langle 0.5, 5 \rangle$

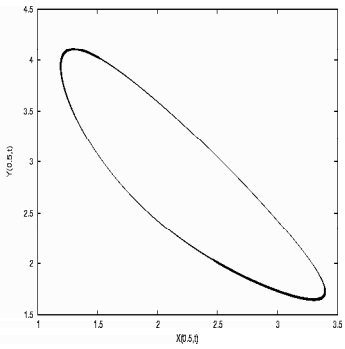

(d) $L = 1.3, \quad t \in \langle 45.5, 50 \rangle$

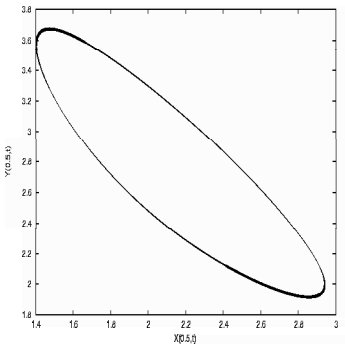

(e) $L = 1.57, \quad t \in \langle 45.5, 50 \rangle$

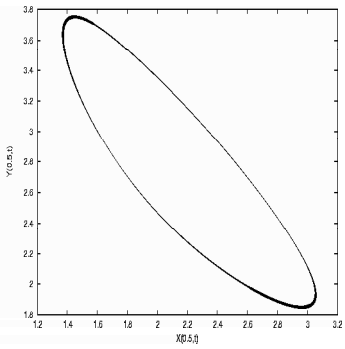

(f) $L = 1.7, \quad t \in \langle 45.5, 50 \rangle$

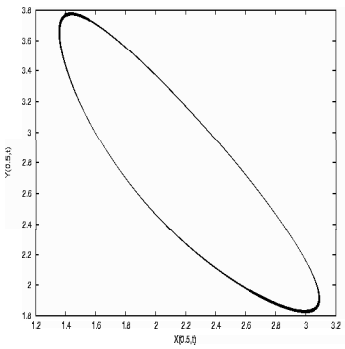

(g) $L = 1.75, \quad t \in \langle 45.5, 50 \rangle$

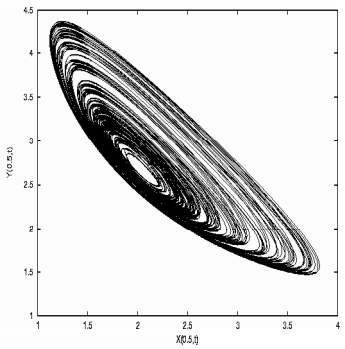

(h) $L = 1.98, \quad t \in \langle 45.5, 50 \rangle$

FIG. 4.3. *Orbits for solutions* $x(0.5,t)$ *and* $y(0.5,t)$ *for various* L, t *denotes time.*

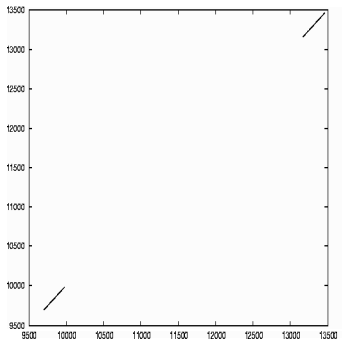

(a) $L = 0.3, \quad t \in \langle 0.05, 1 \rangle$

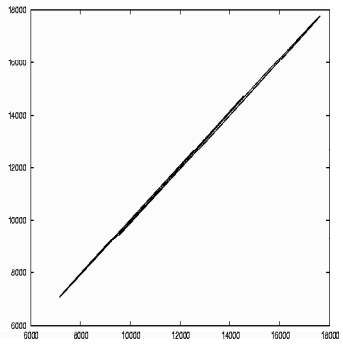

(b) $L = 1.0, \quad t \in \langle 0.5, 5 \rangle$

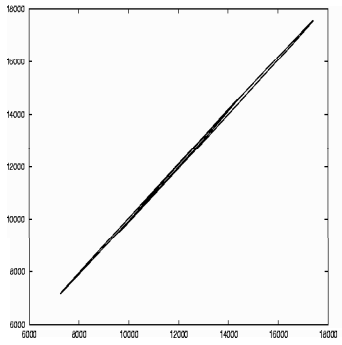

(c) $L = 1.24, \quad t \in \langle 0.5, 5 \rangle$

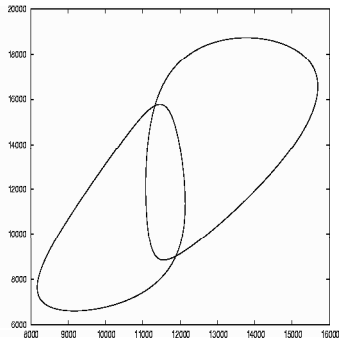

(d) $L = 1.3, \quad t \in \langle 45.5, 50 \rangle$

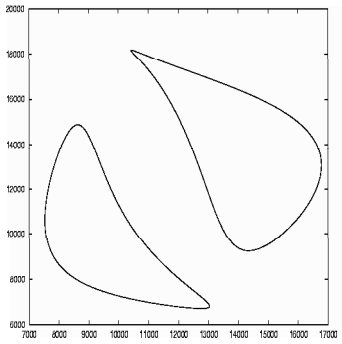

(e) $L = 1.57, \quad t \in \langle 45.5, 50 \rangle$

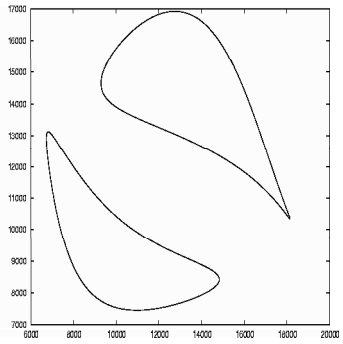

(f) $L = 1.7, \quad t \in \langle 45.5, 50 \rangle$

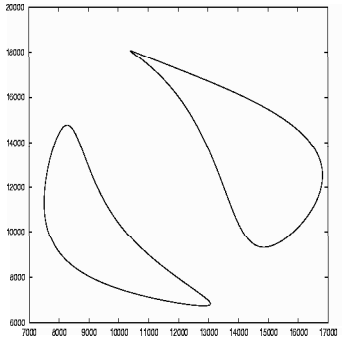

(g) $L = 1.75, \quad t \in \langle 45.5, 50 \rangle$

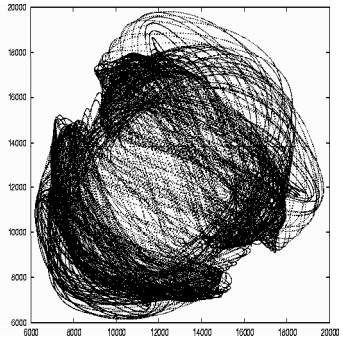

(h) $L = 1.98, \quad t \in \langle 45.5, 50 \rangle$

FIG. 4.4. *Symmetry plots for different* L.

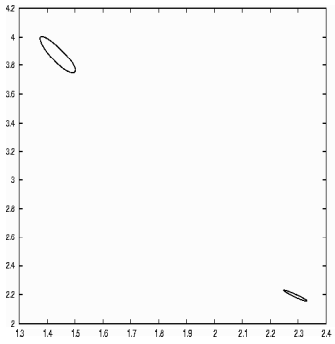

(a) $L = 1.38, \quad t \in \langle 10, 100 \rangle$

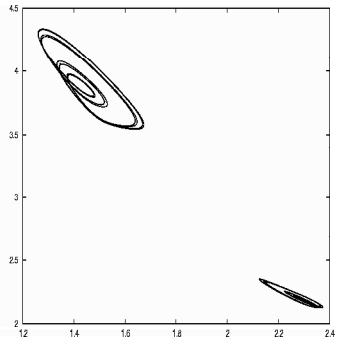

(b) $L = 1.42, \quad t \in \langle 10, 400 \rangle$

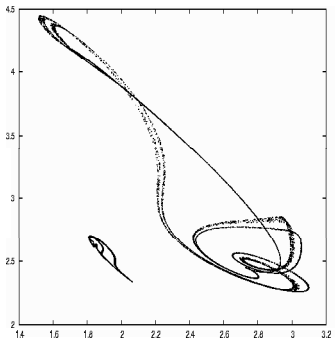

(c) $L = 1.47, \quad t \in \langle 10, 400 \rangle$

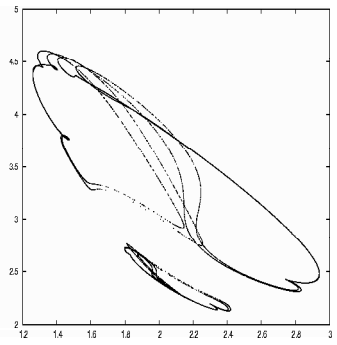

(d) $L = 1.52, \quad t \in \langle 10, 600 \rangle$

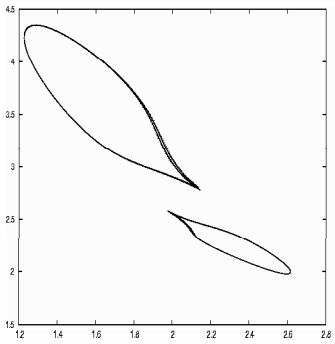

(e) $L = 1.81, \quad t \in \langle 10, 400 \rangle$

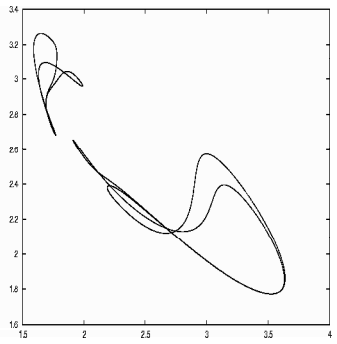

(f) $L = 1.9, \quad t \in \langle 20, 600 \rangle$

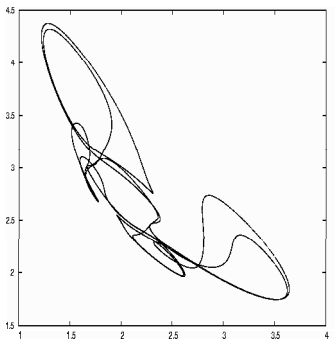

(g) $L = 1.97, \quad t \in \langle 20, 600 \rangle$

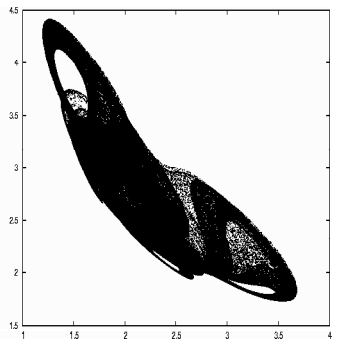

(h) $L = 2.0, \quad t \in \langle 20, 600 \rangle$

FIG. 4.5. *Poincaré intersections with hyperplane* $x(0.6, t) = A$, *points are taken from the centre of reactor tank* $x(0.5, t)$, $y(0.5, t)$.

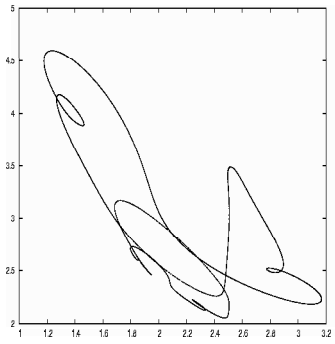

(a) $L = 1.56, \quad t \in \langle 10, 800 \rangle$

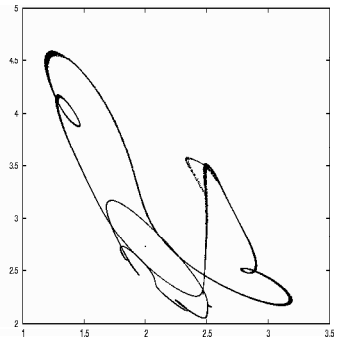

(b) $L = 1.56, \quad t \in \langle 10, 800 \rangle$

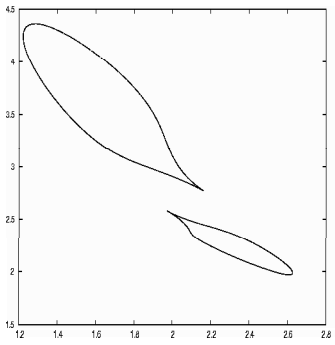

(c) $L = 1.85, \quad t \in \langle 20, 600 \rangle$

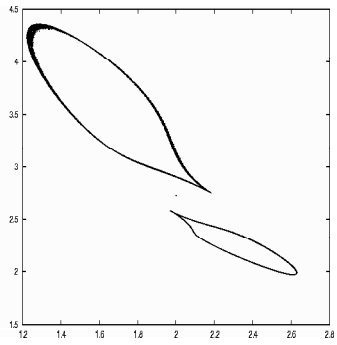

(d) $L = 1.85, \quad t \in \langle 20, 600 \rangle$

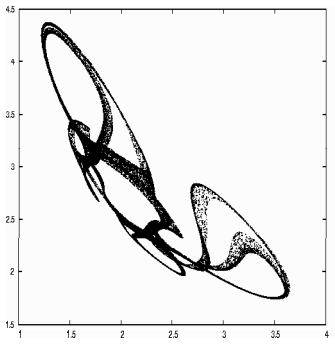

(e) $L = 1.98, \quad t \in \langle 20, 600 \rangle$

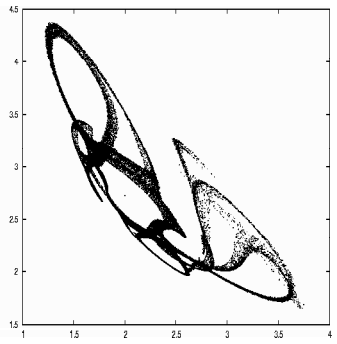

(f) $L = 1.98, \quad t \in \langle 20, 600 \rangle$

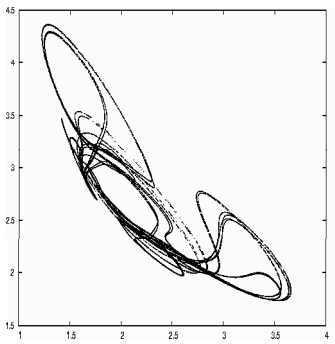

(g) $L = 1.99, \quad t \in \langle 20, 600 \rangle$

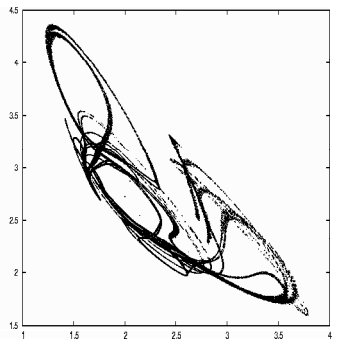

(h) $L = 1.99, \quad t \in \langle 20, 600 \rangle$

FIG. 4.6. *Comparison between linear approximation (on the right side) and the Hénon method (on the left side) for Poincaré intersection.*

[4] J. ŠEMBERA AND M. BENEŠ. *Nonlinear Galerkin method for reaction-diffusion systems admitting invariant regions*, Journal of Computational and Applied Mathematics, Volume, No. 136 (2001),163-176.